



# CHORUS

This is the accepted manuscript made available via CHORUS. The article has been published as:

## Uncommon Deformation Mechanisms during Fatigue-Crack Propagation in Nanocrystalline Alloys

Sheng Cheng, Soo Yeol Lee, Li Li, Changhui Lei, Jon Almer, Xun-Li Wang, Tamas Ungar, Yinmin Wang, and Peter K. Liaw

Phys. Rev. Lett. **110**, 135501 — Published 25 March 2013

DOI: [10.1103/PhysRevLett.110.135501](https://doi.org/10.1103/PhysRevLett.110.135501)

# **Uncommon deformation mechanisms during fatigue-crack propagation in nanocrystalline alloys**

Sheng Cheng,<sup>1\*</sup> Soo Yeol Lee,<sup>1</sup> Li Li,<sup>1</sup> Changhui Lei,<sup>2</sup> Jon Almer,<sup>3</sup> Xun-Li Wang,<sup>4</sup> Tamas Ungar,<sup>5</sup>  
Yinmin Wang,<sup>6\*</sup> Peter K Liaw<sup>1</sup>

<sup>1</sup> *Department of Materials Science and Engineering, University of Tennessee, Knoxville, TN  
37996, USA*

<sup>2</sup> *Department of Materials Science and Engineering, University of Illinois, Urbana, IL 61801, USA*

<sup>3</sup> *X-ray Science Division, Argonne National Laboratory, Argonne, IL 60439, USA*

<sup>4</sup> *Department of Physics and Materials Science, City University of Hong Kong, 83 Tat Chee  
Avenue, Kowloon, Hong Kong*

<sup>5</sup> *Department of Materials Physics, Eötvös University, Budapest H-1518 POB, Hungary*

<sup>6</sup> *Physical and Life Sciences Directorate, Lawrence Livermore National Laboratory, Livermore,  
CA 94550, USA*

\*Emails : scheng.msg@gmail.com; ymwang@llnl.gov

## ABSTRACT

The irreversible damage at cracks during the fatigue of crystalline solids is well-known. Here we report on *in-situ* high-energy X-ray evidence of reversible fatigue behavior in nanocrystalline NiFe alloy both in the plastic zone and around the crack-tip. In the plastic zone, the deformation is fully recoverable as the crack propagates, and the plastic deformation invokes reversible interactions of dislocation and twinning in the nano-grains. But around the crack-tip lies a regime with reversible grain lattice re-orientation promoted by change of local stress state. These observations suggest unprecedented fatigue deformation mechanisms in nanostructured systems that are not addressed theoretically.

PACS numbers: 62.20.me, 62.20.F-, 61.46.Hk

The accumulation of damage is a phenomenon occurring ubiquitously in various crystalline solids under cyclical stresses. In such processes, crack or void nucleation is initiated at structural singularities, but propagation causes the eventual failure. In polycrystalline materials, whether a crack propagates through grains or along grain boundaries (GBs), plasticity is induced ahead of the crack-tip, in a region called “plastic zone (PZ)” [1]. Under classic elastic-plastic framework, the plasticity is modeled with anisotropic dislocation glide on material-dependent slip systems [2]. As the crack advances, the dislocation debris generated in the PZ is permanently left behind, leading to broadened peaks when examined by diffraction techniques [3]. Recent studies demonstrate that the fatigue crack growth in nanocrystalline (NC) metals (with grain-size <100nm) is much faster than that in coarse-grained (CG) counterparts [4], suggesting different near-tip deformation mechanism and crack closure characteristics in NC metals. *In-situ* transmission electron microscopy (TEM) indicates that the concentrated local strain/stress at a crack-tip could cause extensive deformation in NC metals; e.g., dislocations, micro-twinning, or GB sliding/migration; but these activities are irreversible in thin TEM samples due to different stress state compared to those in real-life fatigue [5-7]. The question on what exactly happens in the vicinity of a fatigue crack-tip in *bulk* NC materials remains unknown. Here using a micron-size high-energy X-ray beam to overcome the challenging issues of millimeter-sized samples and site-specific deformations, we probe the local structures around a fatigue crack-tip *in-situ* in a NC Ni-Fe alloy and report revocable near-tip fatigue deformation.

NC Ni-20wt.% Fe alloy was synthesized by pulse electrodeposition. TEM shows that the grains are ~10-20nm with some growth twins [see [Fig. S1, Supplemental Material \(SM\)](#)]. Using a miniature compact-tension (CT) specimen with crack length of 8mm (prepared after 1,783 cycles under  $P_{\max}=2020\text{N}$ ,  $P_{\min}=20.2\text{N}$ ,  $R=0.01$ , and frequency of 10Hz at room temperature in air ([Fig. S2, SM](#)), we started to map out an area of  $1\times 1\text{mm}^2$  around the crack-tip at a lower load level  $P_L$

(=20.2N, corresponding to a stress intensity  $K$  of  $0.3\text{MPa}\cdot\text{m}^{1/2}$ ) and a higher load level  $P_H$  (=1kN and  $K$  of  $14.7\text{MPa}\cdot\text{m}^{1/2}$ ) respectively, with a beam-size of  $50\times 50\mu\text{m}^2$ . Figs. 1(A-F) show the lattice strain distribution, peak width [full width at half maximum – FWHM of (111) peak], and intensity ratio of  $I_{111} / I_{200}$  in the loading direction (LD). First, at  $P_L$  [Fig. 1(ABC)], significant compressive strain (in blue) is generated around the crack-tip, with small tensile strain (in red) ahead of the crack-tip, Fig. 1A. The compressive strain is most prominent in an area of  $\sim 0.2\times 0.5\text{mm}^2$  (width $\times$ length) spanning the crack-tip. Surprisingly, there is a significant peak width reduction around the crack-tip concomitant with the compressive strain, Fig. 1B, contrary to peak width broadening by plastic deformation in conventional materials. Additionally, although the crack runs across half the specimen, as indicated by the white dash lines, the large compressive strain terminates abruptly at  $\sim X=780\mu\text{m}$  at both load levels, as marked by the arrow in Fig. 1A (the X-Y coordinates define the mapping area around the crack-tip, and  $X=780\mu\text{m}$  happens to be the boundary where the stress state changes). After that, the lattice strain rises back to near zero. Intriguingly, the reduced FWHM recovers at  $X>780\mu\text{m}$  as well, Fig. 1B. In the same sample, substantial tensile strain ( $\sim 10^{-3}$ ) is developed at  $>\sim 0.3\text{mm}$  ahead of the crack-tip when the load is raised to  $P_H$ , immediately after the measurements at  $P_L$ , Fig. 1D and Fig. S3 (note that the crack had almost no growth at both load levels). The PZ portrayed by the kidney-shaped tensile strain field ahead of the crack-tip exhibits peak broadening, but around the crack-tip, both the compressive strain and the reduced FWHM are retained, Fig. 1D and 1E. Again, at  $X>780\mu\text{m}$  where the strain is near zero, the FWHM is no longer sharpened. Under both  $P_L$  and  $P_H$ , the reduced FWHM matches perfectly the compressive strain field. This agreement is also reflected in the relative peak intensities: under both  $P_L$  and  $P_H$ , the intensity ratio of  $I_{111} / I_{200}$  is lower around the crack-tip, which spatially corresponds to the compressive strain field and the reduced FWHM,

Fig. 1C and Fig. 1F. The decreased  $I_{111}/I_{200}$  suggests a higher ratio of grains with  $\langle 200 \rangle$  orientation but lower  $\langle 111 \rangle$  orientation in LD, i.e., a change of grain orientation. In transverse direction (TD), reduced FWHM is observed, matching with the strain field around the crack-tip, although tensile strains dominate in the PZ and around the crack-tip, Fig. S4. A similar pattern of  $I_{111}/I_{200}$  is observed in TD.

Mapping suggests two important types of reversible deformation. In the PZ, the FWHM changes from broadened to recovered from  $P_H$  to  $P_L$ , as the tensile strain surges and ebbs, Fig. 1B and 1E. This reversibility marches with the PZ during crack propagation. Around the crack-tip, however, another type of reversibility exists. Although the FWHM remains persistently reduced around the crack-tip (at  $\sim 400\mu\text{m} < X < 780\mu\text{m}$ ), the peak sharpening becomes nearly negligible at  $X > 780\mu\text{m}$ , and  $I_{111}/I_{200}$  is almost similar to that far away from the crack. Note that the FWHM was also reduced when the crack-tip was with this portion of material ( $X > 780\mu\text{m}$ ). But once the stress is released as the crack-tip advances, the FWHM (and the intensity ratio) immediately rises back, to a value similar to that undeformed, indicating that the deformation in this piece of material around the crack-tip is reversed. Both types of reversible behavior are demonstrated in a second NC sample in *in-situ* crack propagation.

The reversible near-tip deformation in NC samples is in stark contrast to that in CG materials. For reference, we conducted near-tip mapping by neutron scattering using a CG Ni-based Superalloy [grain-size  $\sim 90\mu\text{m}$ , single-phase face-centered-cubic (FCC)]. Coarsening NC NiFe alloy for comparison through heat treatment was not adopted due to new phase formation and other complications like brittleness in electrodeposited NC materials [8, 9]. Fig. 2 compares the near-tip distributions of FWHM and the lattice strain (in LD) along the crack path in NC NiFe and CG Superalloy. For both materials, compressive stress is around the crack-tip, while tensile stress is

with the PZ ahead of the crack-tip. In NC sample, the variation of FWHM harmonizes with that of the strain change, Fig. 2A. By contrast, despite the similar stress state, peak broadening was constantly demonstrated both in the PZ and around the crack-tip in CG sample until far ahead of the crack-tip (~16mm), Fig. 2B. Similar phenomena were observed in a CG austenitic stainless steel sample (also with FCC structure) with a grain-size of ~60 $\mu$ m, Fig. S5. These prototype experiments in CG samples witness no reversibility, attesting unique deformation mechanisms in NC materials.

To gain further insight, in a second NC Ni-Fe CT specimen we focus the X-ray beam (100 $\times$ 100 $\mu$ m to shorten exposure time) at a fixed location (at ~2mm ahead of the crack-tip) while forcing the crack grow. The deformation is continuously tracked, as the crack-tip propagates until it passes the beam site by ~5mm (a total growth of ~7mm). Fig. 3A depicts the evolution of lattice strain and (111) FWHM (in LD) as a function of elapsed time. Before the X-ray beam makes contact with the PZ, the FWHM stays nearly constant (elastic deformation), while the lattice strain gradually increases due to the increasing stress intensity. At the moment the PZ being hit (at ~8 $\times$ 10<sup>3</sup>sec), a tensile strain increases rapidly, and the FWHM spikes. As shown in Inset (a) of Fig. 3A, the strain rise precedes slightly that of FWHM, and the FWHM starts to increase only after a critical value of strain,  $\epsilon_c$ , is attained, defined by line I in Inset (a). This critical strain signals yielding (as the rapid increase of FWHM must be induced by plasticity). The lattice strain declines precipitously after the peak, but the drop of FWHM does not happen until the strain down to a value almost equal to  $\epsilon_c$ , as marked by line II in Inset (a). Thereafter, the FWHM steadily decreases with the strain. When the strain falls down to zero, defined by line III, the FWHM settles to the pre-deformation level, as pointed by a horizontal arrow in Fig. 3A. The FWHM is further reduced around the crack-tip accommodating the emergence of the compressive strain. Near the end of the compressive strain regime, the FWHM starts to recover due to the strain relaxation. A

reduced  $I_{111} / I_{200}$  is also observed corresponding to the reduced FWHM, Inset (b) in Fig. 3A. These observations agree with the near-tip mapping in Fig. 1.

The reversible near-tip deformation is uncovered from the evolution of the FWHM. Our peak profile analysis suggests that both dislocations and twinning are active. Fig. 3B depicts the evolution of dislocation density ( $\rho_d$ ) and twinning probability during crack growth. It is interesting that in the PZ (between I and III), the dislocations demonstrate an opposite evolving trend to twinning. Except for the initial increase of twin density ( $\rho_{tw}$ , when the yield stress is reached at line I), the twin probability reduces as  $\rho_d$  increases between line I and line II (Note that the dashed lines in Fig. 3B are at the same moments as these in Fig. 3A). At line II,  $\rho_d$  reaches maximum, while  $\rho_{tw}$  to minimum. After that, as the  $\rho_d$  starts to decrease, the increase of  $\rho_{tw}$  immediately commences (between line II and line III). Extraordinarily, at line III, which marks the moment with zero strain and zero peak-broadening, both  $\rho_d$  and twinning probability restore to their pre-deformation levels, suggesting a reversible process. Moreover, the opposite trend suggests that the enhancing dislocation activities may contribute to the loss of  $\rho_{tw}$  (measured by the reduced twin probability), i.e., dislocation-promoted detwinning, as suggested by experiments and simulations [10-15]. But the loss of twins recovers once the dislocations retreat. After line III enters the area around the crack-tip - a regime with compressive strains (also reduced FWHMs). Across this regime, the  $\rho_d$  drops and then rises in parallel to the FWHM, but the twin probability stays at a level lower than the pre-deformation, with minor changes. The variation of both  $\rho_d$  and twin probability is less appreciable as in the PZ, a marked difference due to the changed stress state. Nevertheless, the change of intensity ratio remains evident in this regime, indicating significant grain re-orientation.

To elucidate how the grain re-orientation accounts for the reversible deformation around the crack-tip, we sectioned TEM specimens from the regime with reduced FWHM (where compressive strain is present) using focused-ion-beam. Examinations reveal grains >100nm that

were not present in the as-deposits; these coarsened grains are located near the crack edge, Fig. 4A. Fig. 4B shows a representative coarsened grain of ~150nm elongated along the crack surface. Within the grain, contrast induced by dislocations is revealed. In addition, many originally large-angle GBs have drifted into small-angle GBs, as exemplified by Fig. 4C. Careful examination suggests that the coarsened grains contain many sub-grains with dislocations formulating the boundaries, Fig. 4D. Moreover, the sub-grains size is roughly the grain-size prior to deformation. The evidences suggest that the coarsened grains are formed through grain lattice re-orientation [6, 16]. The interaction of dislocations with twins can sometimes be encountered, as exemplified in Fig. 4E. In some grains, the growth twins disappeared perhaps under the influence of high stress near crack-tip, while deformation twinning can be traced in other grains [17, 18]. By contrast, the grain coarsening is not observed where the stress field diminished (for instance, at  $X > 780\mu\text{m}$ ). These observations support the results by *in-situ* X-ray diffraction experiment, and suggest complex behavior of NC systems during the fatigue.

The reversible near-tip plasticity in NC materials is scientifically significant. In ductile materials, fatigue crack propagation is known to be accommodated by crack blunting and re-sharpening upon loading-unloading, while the blunting is accomplished through dislocation hardening by irreversible shear on their slip-systems [19-22]. In our NC specimens, although dislocations are active in the PZ, the crack blunting may hardly be fulfilled due to the lack of effective dislocation hardening in nano-grains [23]. The fast crack growth rate and smooth fracture surface in our NC samples support the hypothesis, Figs. S6 & S7. Conversely, the opposite change of twinning vs. dislocations in the PZ hints that the transient dislocations could interact with twinning during loading cycles, perhaps caused by the emitting dislocations from GBs [24], but the reversible character may not provide the hardening. Around the crack-tip, the reversible grain lattice re-orientation represents another deformation mode that challenges the traditional concept

of near-tip plasticity. A large grain containing domains with the original nano-grains suggests that coarsening should occur through lattice re-orientation of the nano-grains under the stress field. Consequently, lattice misorientation between nano-grains minimizes, forming a united grain. With the stress field set free, the building domains rotate back to their original orientation, reversing the coarsening. The fact that a coarsened grain can transform back to the original nano-grains under the influence of stresses is unexpected and hints that the deformation is predominantly carried out at the boundaries of nano-grains, the evidence of which is collected in the *post-mortem* TEM studies. This is in contrast to not only CG samples where the deformation is predominated by the dislocations leading to peak width broadening, but also to the irreversible grain growth through the mechanically-driven GB migration reported in other NC samples [5, 25].

### **Acknowledgements**

The authors thank Prof. J.R. Weertman for her helpful comments. Financial support was by the NSF Grants No. DMR-0421219 and No. DMR-0231320. The APS was supported by the U.S. DOE (DE-AC02-06CH11357). The work at LLNL was supported by the U.S. DOE (DE-AC52-07NA27344).

## References

- [1] R. W. Hertzberg, *Deformation and fracture mechanics of engineering materials* (John Wiley & Sons Inc., 1996), 4th edn.
- [2] R. O. Ritchie, *International Journal of Fracture* **100**, 55 (1999).
- [3] B. E. Warren, *X-ray diffraction* (Dover Publications Inc., New York, 1969).
- [4] T. Hanlon *et al.*, *Scripta Mater.* **49**, 675 (2003).
- [5] T. J. Rupert *et al.*, *Science* **326**, 1686 (2009).
- [6] Z. W. Shan *et al.*, *Phys. Rev. Lett.* **100** (2008).
- [7] M. Ke *et al.*, *Nanostruct. Mater.* **5**, 689 (1995).
- [8] L. Li *et al.*, *Acta Mater.* **57**, 4988 (2009).
- [9] Y. M. Wang *et al.*, *Scripta Mater.* **51**, 1023 (2004).
- [10] Y. D. Wang *et al.*, *Adv. Eng. Mater.* **12**, 906 (2010).
- [11] J. Wang *et al.*, *Acta Mater.* **58**, 2262 (2010).
- [12] S. Y. Hu *et al.*, *Acta Mater.* **58**, 6554 (2010).
- [13] B. Q. Li *et al.*, *Phys. Rev. Lett.* **102** (2009).
- [14] S. Cheng *et al.*, *Adv. Mater.* **21**, 5001 (2009).
- [15] D. H. Warner *et al.*, *Nat. Mater.* **6**, 876 (2007).
- [16] M. Jin *et al.*, *Acta Mater.* **52**, 5381 (2004).
- [17] Y. T. Zhu *et al.*, *Prog. Mater Sci.* **57**, 1 (2012).
- [18] C. J. Shute *et al.*, *Acta Mater.* **59**, 4569 (2011).
- [19] F. Cleri *et al.*, *Phys. Rev. Lett.* **79**, 1309 (1997).
- [20] J. Weertman, *Philos. Mag. A* **43**, 1103 (1981).
- [21] R. M. N. Pelloux, *Asm Transactions Quarterly* **62**, 281 (1969).
- [22] P. Neumann, *Acta Metall.* **17**, 1219 (1969).

- [23] I. A. Ovid'ko *et al.*, *Acta Mater.* **58**, 5286 (2010).
- [24] H. Van Swygenhoven *et al.*, *Phys. Rev. B* **66** (2002).
- [25] K. Zhang *et al.*, *Appl. Phys. Lett.* **87** (2005).

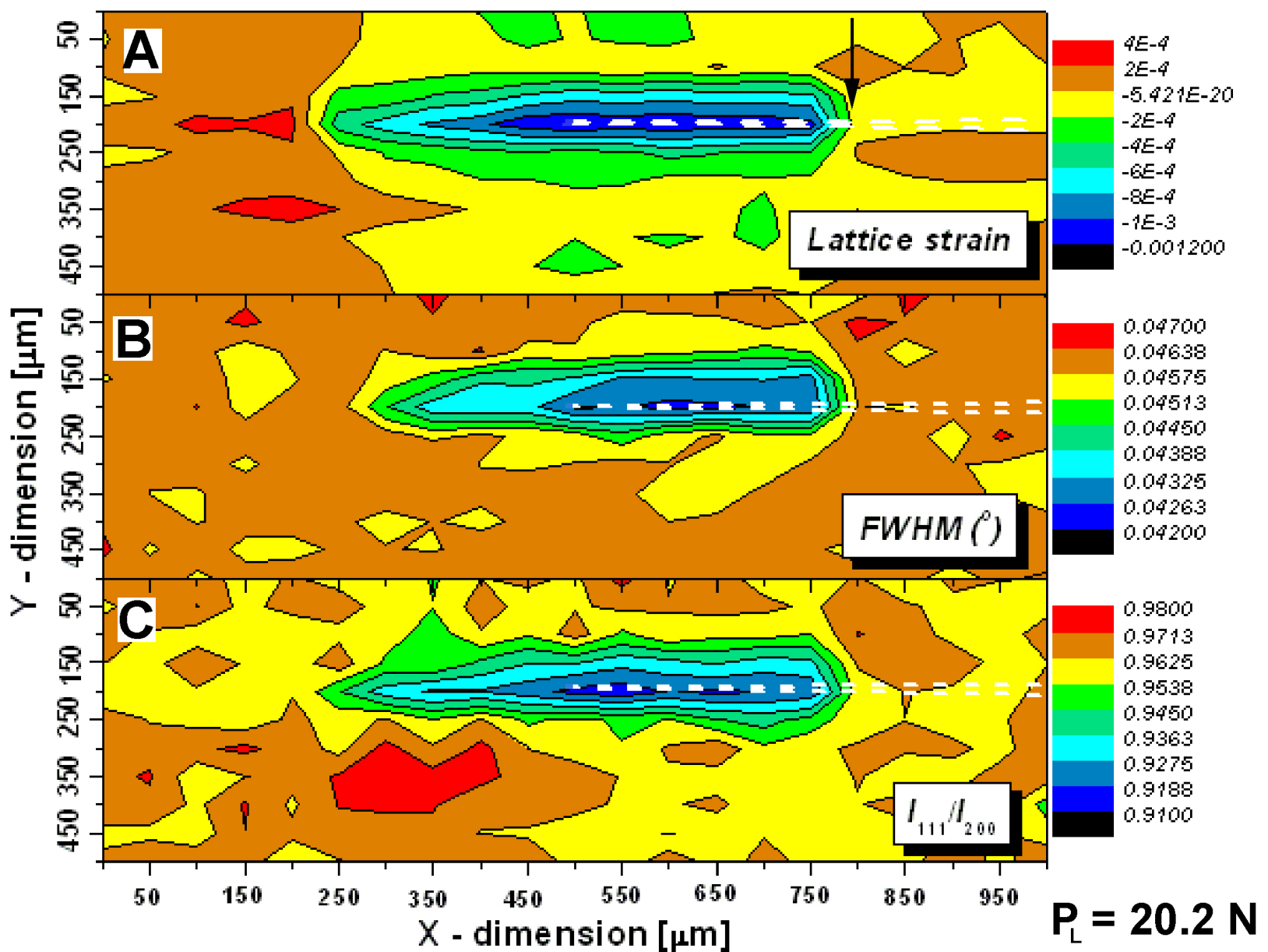
## Figure Captions

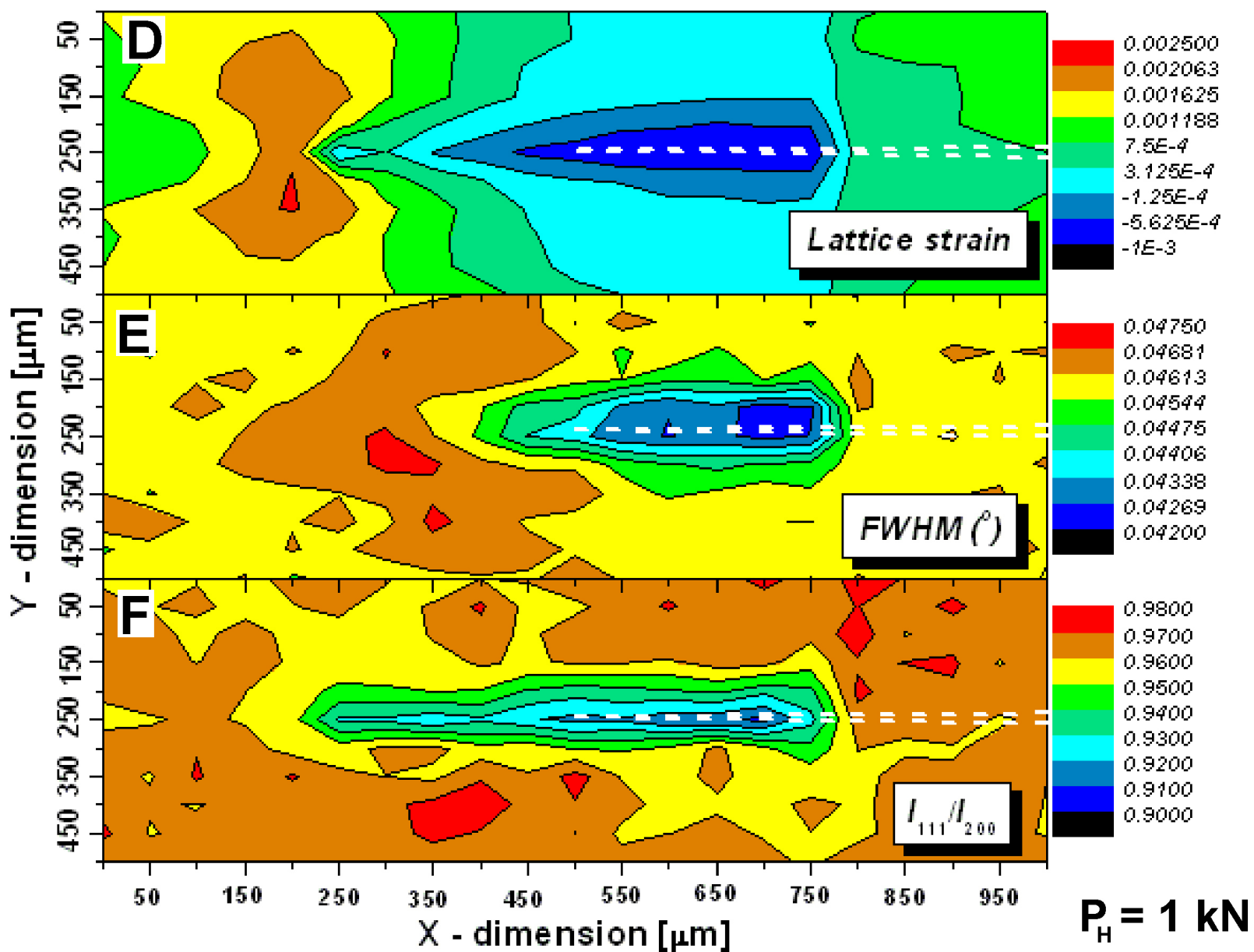
**Fig. 1.** The lattice strain, FWHM-(111), and  $I_{111}/I_{200}$  revealed in LD at  $P_L$ , (ABC) and  $P_H$  (DEF – measurements followed ABC immediately at the same area): (A) high compressive strain generated around the crack-tip, but small tensile strain ahead of the crack-tip; (B) FWHM greatly reduced around the crack-tip; (C) Decreased  $I_{111}/I_{200}$  corresponding to the reduced FWHM and compressive strain; (D) PZ registered with tensile strain ahead of the crack-tip, but compressive strain around the crack-tip; (E) FWHM broadened in the PZ, but sharpened around the crack-tip; (F) Reduced  $I_{111}/I_{200}$  around the crack-tip.

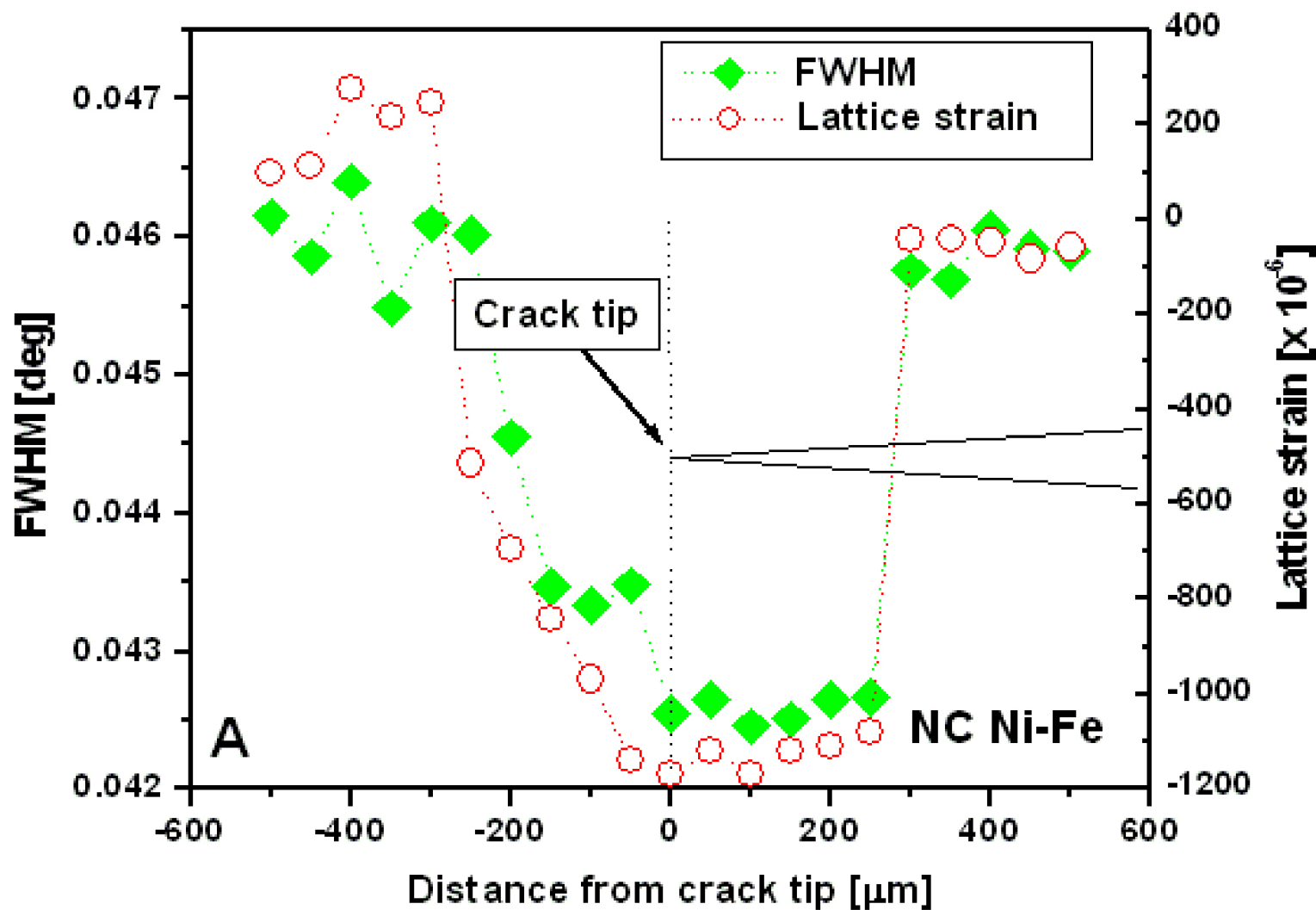
**Fig. 2.** The lattice strain, FWHM-(111) in LD along the crack path in: (A) NC NiFe at  $P_L$ ; (B) CG Ni-based C-2000 Superalloy as-fatigued. In both NC NiFe and CG Ni-alloy, compressive strain is around the crack-tip, with tensile strain in the PZ. In CG sample, peak broadening is in both the PZ and around the crack-tip, but peak sharpening is around the crack-tip in NC sample, which can be recovered when the stress diminishes.

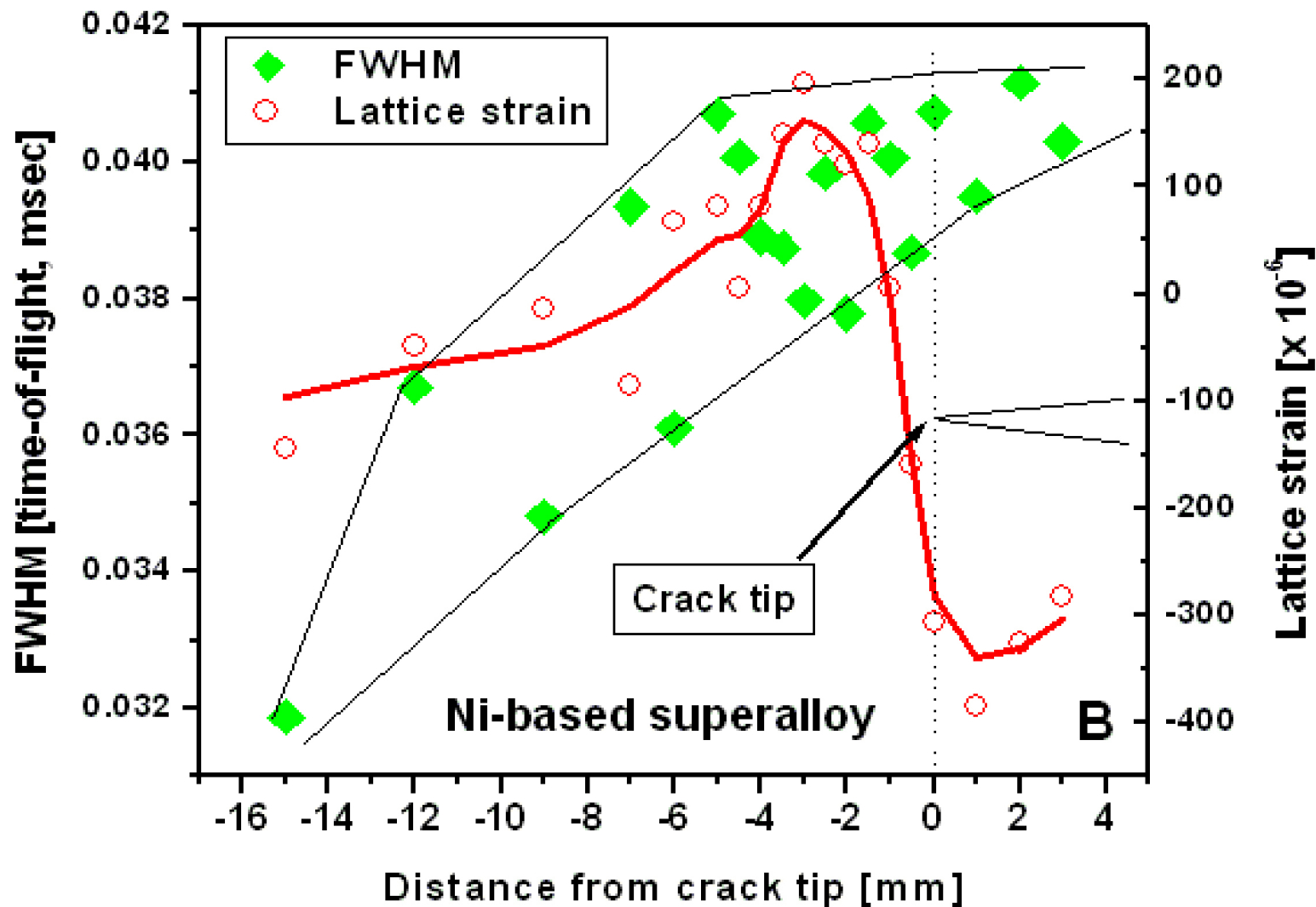
**Fig. 3.** (A) The evolution of FWHM-(111) and strain during *in-situ* crack propagation. Before I: the elastic deformation before the PZ being detected; I-III: the deformation in the PZ; after III: compressive strain with peak sharpening around crack-tip. Inset (a) is a close-up view of PZ, and Inset (b) shows  $I_{111}/I_{200}$  in correlation with FWHM. (B) The evolution of  $\rho_d$  and twin probability during *in-situ* crack growth.

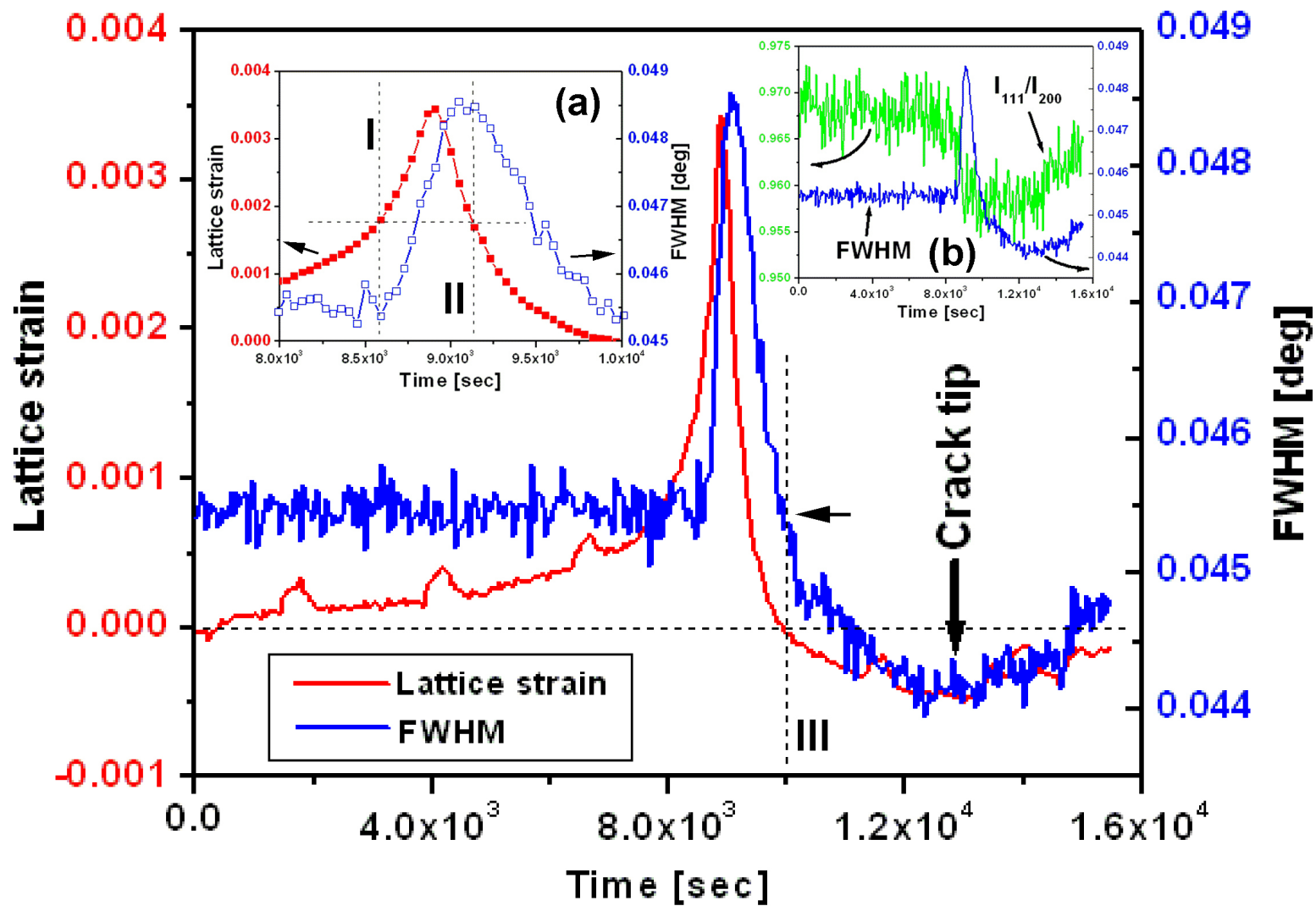
**Fig. 4.** (A) Scanning-TEM image shows coarsened grains near the crack edge cut from where the compressive strain in LD; (B) High-resolution-TEM image shows the typical structure of a coarsened grain; (C) Small-angle GBs are revealed due to grain lattice re-orientation; (D) Example of two nano-grains merge into a large grain; (E) Dislocations interact with twins.

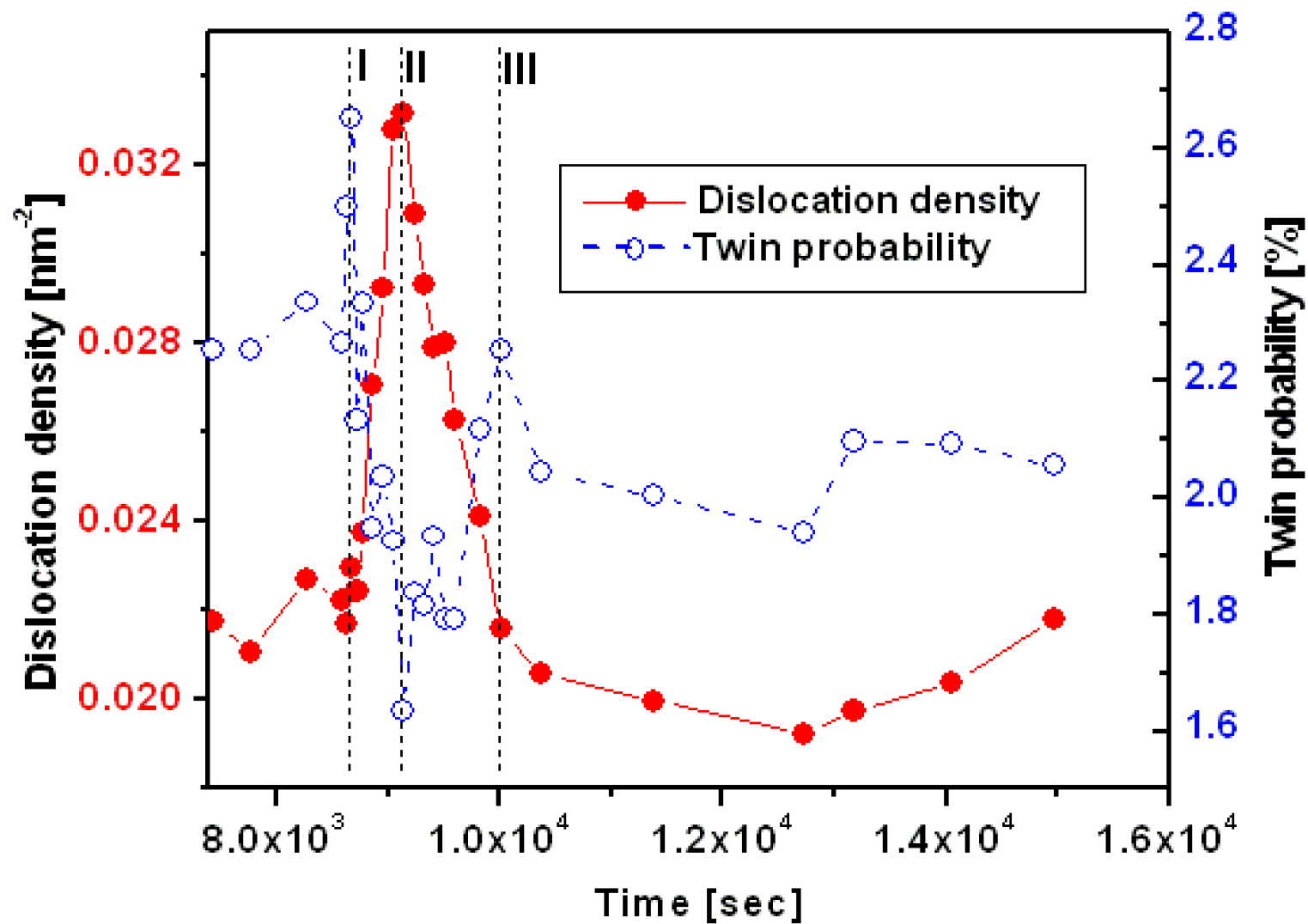






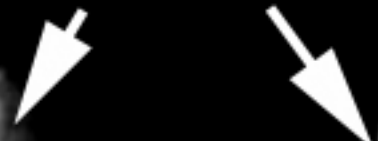


**A**

**B**

**A**

**Crack edge**



**100 nm**

